Spring 2018

An Integration Setup if the in-situ Mass and Spectroscopic Analysis for Volatile Liquids or Solids

Kolton K. Jones
Western Kentucky University, kolton.jones866@topper.wku.edu

AN INTEGRATION SETUP OF THE IN-SITU MASS AND SPECTROSCOPIC
ANALYSIS FOR VOLATILE LIQUIDS OR SOLIDS

A Thesis
Presented to
The Faculty of the Department of Physics and Astronomy
Western Kentucky University
Bowling Green, Kentucky

In Partial Fulfillment
Of the Requirements for the Degree
Master of Science

By
Kolton Kenneth Jones

May 2018

AN INTEGRATION SETUP OF THE IN-SITU MASS AND SPECTROSCOPIC ANALYSIS FOR VOLATILE LIQUIDS OR SOLIDS
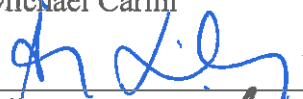
Date Recommended July 20, 2017

_____
Yan Cao, Director of Thesis

_____
Michael Carini

_____
Ali Er

_____
Ivan Novikov

_____
Sanju Gupta

_____   7/25/17
Dean, Graduate Studies and Research   /   Date

I dedicate this thesis to my parents, Kenneth and Racheal Jones, who have inspired me.

TABLE OF CONTENTS

ABSTRACT

AN INTEGRATION SETUP OF THE IN-SITU MASS AND SPECTROSCOPIC
ANALYSIS FOR VOLATILE LIQUIDS OR SOLIDS

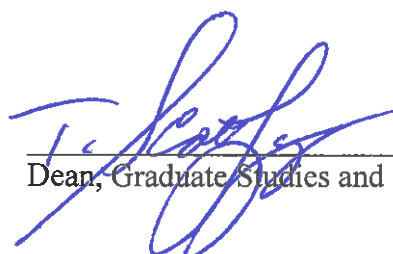Kolton Jones   May 2018   25 Pages

Directed by: Yan Cao, Michael Carini, Ali Er, Ivan Novikov, and Sanju Gupta

Department of Physics and Astronomy   Western Kentucky University

        To help address the growing need for more and better sensors, an attempt was made to produce an in-situ mass and spectroscopic analysis of liquid and solid samples, to characterize samples and sensors. Spectroscopic analysis consisted of Raman and FTIR where mass measurements were carried out. The sample or sensor's holder would allow for spectroscopic analysis as well as expose the sample to high temperatures and various chemicals. While Raman and FTIR were successful in producing reliable and consistent data, the constructed watt balance was not. This failure was a result of eliminate vibrational noise.

Chapter 1

Introduction

The Department of Homeland Security (DHS)'s mission: The vision of homeland security is to ensure a homeland that is safe, secure, and resilient against terrorism and other hazards. To address the mission, DHS relies on sensors for detecting chemicals, explosives, and drugs. These sensors will be exposed to a variety of different environments; for example, wearable sensors and drone sensors, carbon monoxide sensors, hall effect sensors, and humidity sensors.

Environmental conditions need to be considered when designing sensors. Neglecting to do so can affect the sensor's accuracy. Sensors utilized in new environments may malfunction. Thus, the characterization of sensors in different environments is critical to ensuring the information gathered from implemented sensors is accurate. This thesis is to partially develop an in-situ sensor - chemical characterization platform. The platform presented in this thesis can perform simultaneous FTIR, Raman spectroscopy, and measure mass as a function of time.

Theory

In-situ monitoring of a sample from three criteria mass, Infrared Spectroscopy, and Raman Spectroscopy in different environments is part of the goal of this thesis. To understand the complexity of the endeavor, a fundamental understanding of the techniques being used is required.

A Watt Balance(WB) is used to measure the mass of an object. The WB is similar to an equal arm balance, except the WB is active while the equal arm balance is passive.

The WB only adds some components to the equal arm balance; most notably a couple solenoids, a system for detecting distance and movement, and a computer.

Kibble, Robinson, & Belliss's (1990) insight reduced the complexity of obtaining accurate mass measurements. Their insight adopted the approach of using virtual power to relate mechanical power to electrical power; thus allowing the ability to relate electrical quantities to mass. The WB is able to measure mass by applying the Lorentz force and the discovery and invention made by Kibble, Robinson, & Belliss (1990). The relationships are expressed in Kibble's insight.

To determine a sample's mass involves implementing two methods: Velocity Mode and Force Mode. As Kibble showed, doing Velocity and Force Modes separately at different times simplifies the process of determining mass. Kibble's Insight:

$$F_z = mg = I\frac{U}{v_z} => mgv_z = IU = \frac{U^2}{R} => m = \frac{IU}{gv_z} \qquad \text{Equation 1}$$

In Equation 1 the symbols are defined in the following: F is force, m is mass, g is the acceleration do to gravity, I is the input current, current in the solenoid, v_z is the vertical velocity, and U is the electric potential.

In both Velocity Mode and Force Mode, two coils will be used: Coil A and Coil B. Coil B will be used as the driving Coil, where current will be inserted into Coil B and the resulting magnetic field will repel Coil B from the magnetic coaxially below it. Coil A will be the measuring coil, where Voltage V and Current I will be monitored. In Equation 1 and Equations 2, B is the magnetic flux density, and L is the length of solenoid. In Equation 1, v is the vertical velocity.

Velocity Mode	$V = BLv$	Equation 2

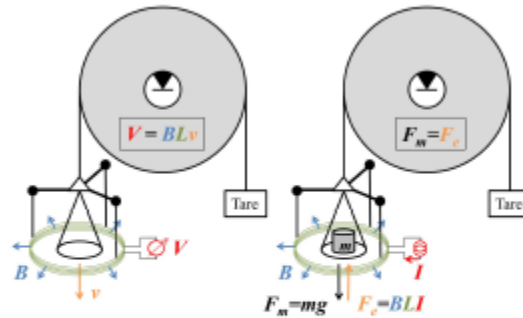| Force Mode	$F = ma = BLI$	Equation 3

FIG. 1. Left: velocity mode. The coil moves vertically in a radial magnetic field and a voltage V is induced. Right: force mode. The upward electromagnetic force generated by the coil opposes the gravitational force exerted by m.

Figure 1(Chao, L. S., et al., 2015)

Velocity Mode

The driving coil is made to produce oscillations in the height of the measuring coil, approximately 1 mm, with various periods. Different velocities will result from the various periods, and Induced Voltages can be recorded, BL.

$$\frac{V}{v} = BL \qquad \text{Equation 4}$$

A solenoid, of length L, is moved vertically with velocity v through a magnetic field, flux density B, resulting in an induced voltage across the solenoid.

Force Mode

The measurement coil is brought into stable equilibrium, a is the gravitational acceleration, the driving coil produces Lorentz force to be equal and opposite of the mass

on the coil measurement side, while at the same time the current is being measured in the

measurement coil. Substituting BL that was discovered from Velocity Mode into Force

Mode shown below. Followed by solving for mass.

$$F = ma = (BL)I = (\frac{V}{v})\boldsymbol{I}$$
Equation 5

$$a = g$$
Equation 6

$$m = (BL)I = (\frac{V}{vg})\boldsymbol{I}$$
Equation 7

Infrared Spectroscopy

Infrared spectroscopy, also known as molecule vibrational spectroscopy, uses

infrared light (cm^{-1}) to study functional groups of chemicals and identify chemicals. The

reason infrared spectroscopy is also known as a vibrational spectroscopy is because when

infrared light strikes a molecule, the electric field of the incoming light causes a change

in the electric dipole moment of the molecule, and if the oscillations of the electric dipole

moment match the frequency of the incoming light, it then is absorbed. This, in turn,

causes the molecule to increase its vibrational energy level. The frequency of infrared

light happens to be absorbed since it matches the molecules natural frequencies. The

energy of the infrared light is enough to increase the vibrational and or rotational energy

levels of molecules, but not enough to cause an electronic energy level transition.

Infrared spectroscopy is only suited for all molecules that fit the criteria of infrared

spectroscopy's selection rules.

Selection Rules for vibrational transitions

- Vibrations must produce a change in electric dipole moments of molecules

- Allowed Infrared Transitions: $\Delta v = \pm 1$ $\boldsymbol{\Delta E_{v \to v+1}} = hv = \hbar\omega$

- Overtone Infrared Transitions: $\Delta v = \pm 2, \pm 4, \pm 6 \dots$

Explaining the selection rules

The incident infrared light must interact with a normal mode of a molecule that has an oscillating electric dipole moment at the same frequency as the incident infrared light.

Allowed Infrared Transitions are based on the incorrect assumption the molecules oscillate as a perfect harmonic oscillator.

Overtone infrared transitions, forbidden infrared transitions, are allowed since the assumption in the allowed infrared transition is not correct.

Fourier transform infrared spectroscopy (FTIR) is a technique that is used to obtain infrared spectra with high spectral resolution, high spectral accuracy, and a high signal-to-noise ratio. FTIR is typically based on the Michelson Interferometer, with the addition of additional optics, infrared source and detector, and a stepper motor. the FTIR uses wave interference to create an infrared interferogram at the detector and then collected. The interferogram is translated into a spectrum through the Fast Fourier Transform algorithm.

The FTIR used in this setup is based on Fabry-Pérot interferometer (FPI). The FTIR used in this thesis uses a Fabry-Pérot interferometer (FPI) instead of a Michelson Interferometer. FPI makes use of multiple reflections between two closely spaced partially silvered surfaces. Part of the light is transmitted each time the light reaches the second surface, resulting in multiple offset beams that can interfere with each other. A large number of interfering rays produces an interferometer with extremely high resolution, somewhat like the multiple slits of a diffraction grating increase its resolution.

If the FPI-FTIR is going to be used at a different angle other than normal to the source the following is important to consider.
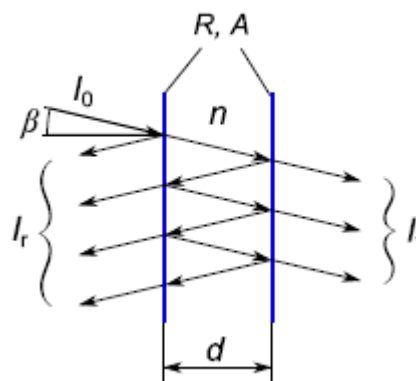
$$\lambda_m = \frac{2\,nd\,\cos(\beta)}{m}$$

Figure 2 (InfraTec, 2014)

Where λ_m has transmitted wavelength, n is the index of refraction of the internal medium of the FPI, β is the angle of normal incidence, m is the interference order (InfraTec, 2014).

Raman Spectroscopy

The Raman Spectroscopy technique uses monochromatic laser light to interact with a sample (solid, liquid, or gas), where most of the light collected is that of laser light elastically scattering off the sample. The other light collected is due to inelastic scattering (Stokes or Anti-Stokes). Stokes scattering occurs when collected light has less energy than the excitation light source, Anti-Stokes scattering occurs when the collected light has more energy that the excitation light source. These shifts in energy occur when the excitation laser source excites the sample molecules in their ground or excited rovibrational state (rotational and vibrational energy level within its given electronic state). This change in the initial and final energy states results in inelastic scattering. The Raman's stokes or anti-stokes scattering is dependent on the dipole polarizability. Scattering involves a momentary (polarized or momentary induced dipole) distortion of the electrons distributed around a bond in a molecule, followed by reemission of the radiation as the bond returns to its normal form.

The Raman Selection rules are like infrared selection rules

1 $\Delta v = \pm 1$

2 Electron polarization changes during vibration

3 Second order notations in the character table indicates Raman-active vibrations.

The Raman shift is directly related to the vibrational energy levels that relate to the inelastic scattering of stokes and anti-stokes scattering. When the oscillating electric field interacts with the sample's electron cloud, the magnitude of Raman Scattering is determined by how easily the electrons move in the response to the electric field.

Chapter2

Apparatus

Initially a LEGO Watt Balance was built to demonstrate how the kilogram might be redefined to have a relationship with Planck's constant. An attempt to replicate the LEGO Watt Balance was undertaken, and the prime objective was to test the feasibility of building a Watt Balance to accurately measure mass and for later expansion into other endeavor.
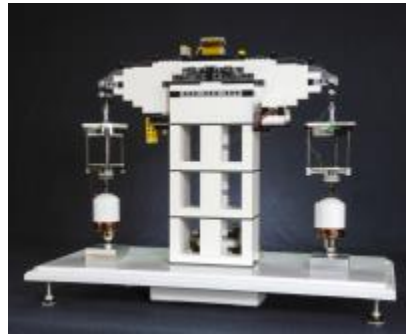
Figure 3 (Chao, L. S., et al., 2015)

Many of the items on the LEGO Watt Balance's parts list were able to be found on LEGO's direct website, eBay for discontinued LEGO items cheaper lasers were bought from Newegg. The unused data acquisition (DAQ) in lab was better that the one used LEGO Watt Balance; additionally, similar neodymium magnets were used instead of the recommended neodymium magnets. It was decided to order the magnetics and lasers, but not LEGO, because many of the needed LEGOs had been discontinued.

The design of the Watt Balance was physically similar as in Figure 3. The Watt Balance has an elevated balancing arm; on each side of the Watt Balance a measuring pan is connected to a solenoid that is concentric to a stationary magnet. For both sides of

the Watt Balance, there are two lasers: one used as a shadow sensor and one for an angle indicator. In this paper, the two lasers were replaced with an interferometer.

The strategy to construct a Watt Balance was to build several balancing systems, balancing arms and fulcrums, and determine which design was the most stable and functional. Different methods for elevating the Watt Balance wre evaluated based on its stability. Different holding pans, sample holders, and coils were constructed and evaluated by their functionality, using a circuit and DAQ to control the two operational modes of the Watt Balance. Several designs were built in SolidWorks to be used as a guide during construction and for presenting.
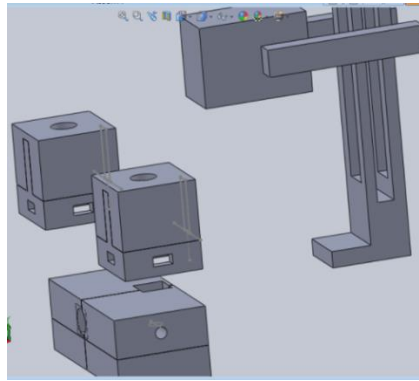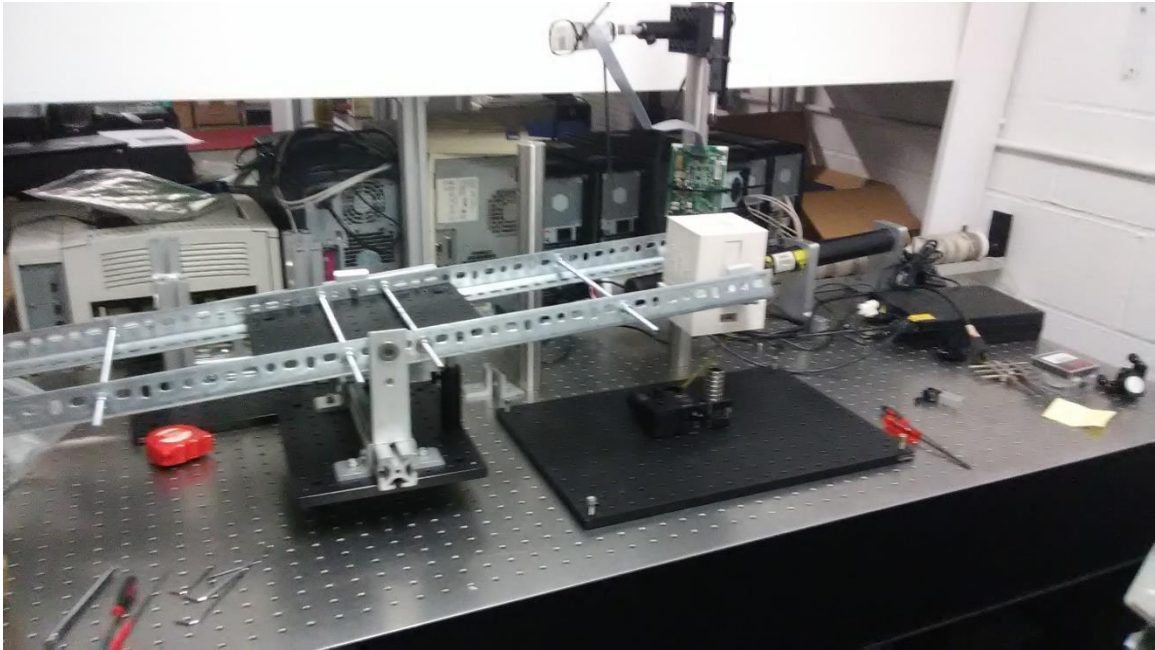

Picture 1

Figure 4

Figure 4 shows one of the last Watt Balance configurations. In this setup, the IR source is mounted inside the sample holder. Additionally, the interferometer is setup and the right-angle mirror is aligned with the mirror mounted inside the sample holer.

The software was written in LABVIEW and the circuit board was made in Eagle and ordered from SEEEDSUDIO. In Velocity Mode the input or driving voltage was with a DC voltage, 0 - 10 V, and the position was detected from the interferometer. The changes of fringe represented the change in distance while the LabVIEW program recorded the time. With the distance and time gathered, velocity was easily determined. In this case, one coil was used to drive the motion. As the input voltage changed so did the height of the non-driven coil. By monitoring the velocity and the driving voltage, voltage/velocity was found. Force Mode uses is driven by a PID program to keep the balance in the nominal position. The current is needed to solve for mass.

The functionality of Velocity Mode and Force Mode depends on the accuracy and reliability of the interferometer. First, the interferometer needs a static measurement before the interferometer can be used to detect displacements.

Before the ordered parts arrived, the LEGO Balance's free control software was evaluated to the conclusion it would work with the current DAQs. The attempts to contact the authors and access to the program's code were unsuccessful.

Three types of fulcrums were used in the place of the recommended LEGO knife edge: loose fitted optical post mount, razor blades, and ball bearing. Using each fulcrum in several different configurations to determine how to best stabilize the Watt Balance, each fulcrum presents their own strengths and weakness. The optical post mount was the first fulcrum and quickest to assemble for use. Using the optical post holder as a fulcrum was inconsistent with the wobbling arm orientation. A guiding wall was implemented to circumvent this issue, but the wall often caught the arm of the Watt Balance and stopped its movement. Since this previous method did not work different attempts was made implementing optical rails from THORLABs that were used and the lever arm of the Watt Balance. This presented its own challenges, but was quickly fixed by using optical posts to limit the rotation of the lever, and the wobble and catching was greatly limited. The wobble at time became only noticeable by shining a light directly under the lever arms and observing the changing of the shadow on a distant wall.

Using the optical rail and the optical post produced more friction than the ideal knife edge. Given the situation, a literature search revealed two alternatives: obsidian and razor blade. Obsidian is not easily functional for this application, though it is sharp, the edge is not straight.

Razor blades have sufficient straightness and sharpness. A razor blade was fixed to the optical rail, with make shift clamps, and used as the fulcrum. Other methods were evaluated and were found to be viable options, but were not used as the make shift clamps were more versatile.

Substituting the Razor blade for the fulcrum was very beneficial. Using a razor blade as the fulcrum maintained the previous benefits of the previous configurations, but with decreased friction. Unfortunately, after few uses the razor blade became more brittle and lost a good deal of sharpness and straightness. Electrical tape was added to cover the blade, resulting in a prolonged the functionality, increased friction, and trivial wobbling. The use of ball bearings as a fulcrum will be elaborated in the future.

Since a suitable fulcrum and balancing arm was found, progress of elevating the Watt Balance was attempted through two different methods: multicable optical posts and two 1.5-inch diameter optical posts.
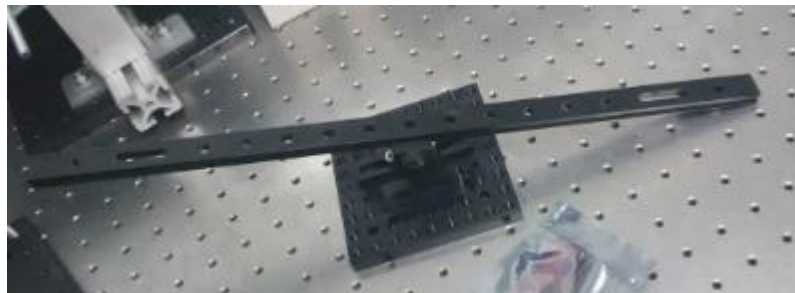

Figure 5 A Watt Balance with a razor blade configuration without the razor blade.

The two 1.5 inch optical posts were placed in close proximity, each having a drilled side mounts. Several attempts were made to fix the Watt Balance between these two posts such that the balance would stable. Differences in tapped holes prevented the optical posts from restricting the wobble of the Watt Balance in this configuration. An

attempt to circumvent this issue, right angle mounting brackets with bread board secured to each provided a horizontal and flat surface to work from. This did improve the ease in which maintenance could be performed, but introduced difficulties and setting the same height. The Watt Balance's arm fell off of the apparatus less frequently.

Three different configurations were tested using the optical posts either using two or four optical posts as mounts. Testing the razor blade with electrical tape fulcrum configuration with each of optical post configurations. The configuration with two optical posts supported a large area bread board where the Watt Balance configuration was placed. Using the two-optical post configuration was easy to assemble and appreciably kept all the benefits of the razor blade with electrical tape fulcrum. The four-optical post configuration showed not observable stability difference, but a larger area bread board was able to be used. The assumptions at the time the larger area bread board would allow for the DAQ, hadow sensor, control board, and to abundant room for potential additional parts.

Figure 6 is shows an elevated test setup.

The first holding pan was fashioned from optical posts, parts paint brushes, round pads of wood. The holder did require that all parts be non-ferrous. The optical posts are made from Aluminum. The holes in the wood pads were drilled by hand power drill or a computer numerical control (CNC) machine. The hand power drilled holes were not as symmetrical, but didn't warp the wood as the CNC machine did when the wood was clamped down. The CNC machine wood pads were used because of the speed and accuracy the holes. The bowing was acceptable since this was a stand in item, but the important parameter is that they are symmetric, non-ferrous and have nearly the same mass. A simple screw was the best choice for securing the pans to the Watt Balance. Mounting the pan on an optical rail slide was disregarded as keeping the pans at equal distance from the axis is extremely important for an equal arm balance.

The current required to control the Watt Balance is greater than the DAQ is designed to deal with. As a result, an additional circuit board is required to handle currents outside the range of the DAQ. The LEGO provided circuit board was designed so the polarity of the system could be changed easily. This was not the intent of the authors attempt to replicate the LEGO Watt Balance, a simplistic circuit design would be used in place of the circuit design provided. The simplistic design consisted of an n-channel transistor and a manually controlled potentiometers and coil.
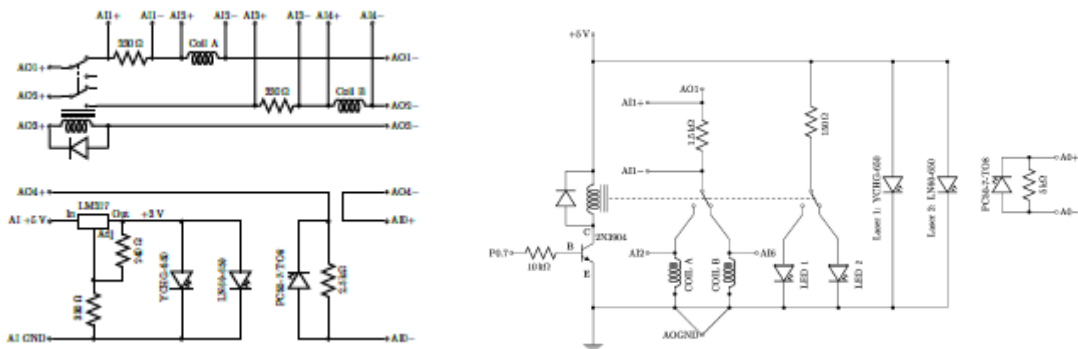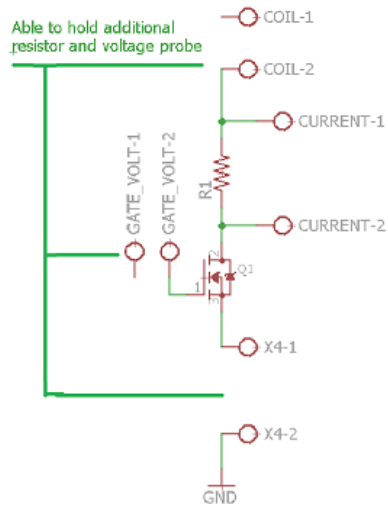
Figure 7   Figure 8

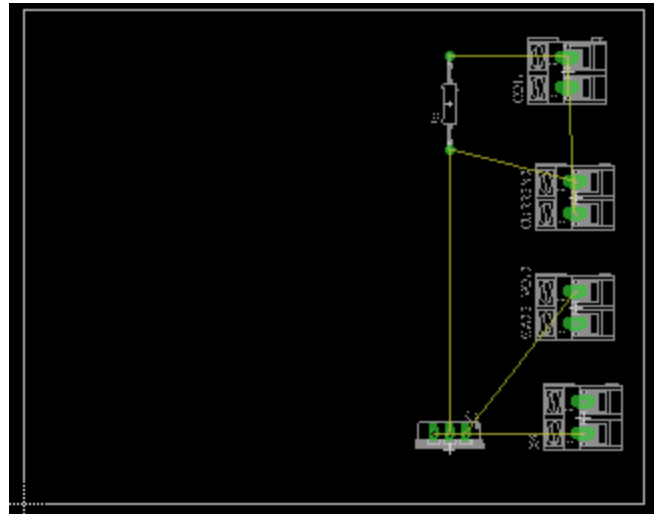

Figure 9   Figure 10

Figure 7 and Figure 8 are the designs that were recommended. Figure 9, Figure 10, Shows the circuit board that was used for this experiment drawn in Eagle.
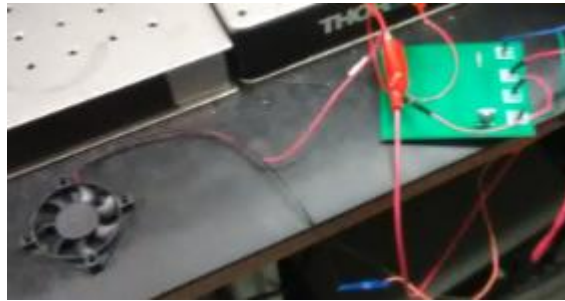

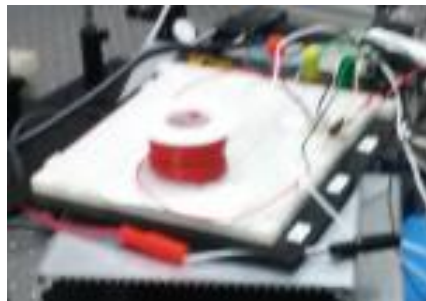Figure 11 shows the Circuit Board being used to control a DC fan.

Figure 12 shows the test circuit board before ordering a printed circuit board.

The first test of the custom circuit board was with a DC fan. A Fan was chosen since if the control board worked the fan would spin and make sound which is easily observable without electrical measurements After several attempts, I was able to control the fan by varying the voltage to the N-channel transistor's gate pin. The same test was done with different hand-held coils. Several would burn out quickly. The current was great enough to burn most of the wires. An additional resistor was added to prevent the wire from burning.

Figure 13

Attempting to use another power supply resulted in the N-channel Transistor from working. After several tests a circuit board was ordered. Once the circuit board arrived it was tested and found it was functional, though the original connectors were not able to be found connecting wires were still soldered on.

A laser interferometer was used to functionally replace the laser needed for angle measurements, and shadow sensor, a photo-gate.

At this point Coils were attached to the Bottom of each pan of the Watt Balance. Then a Magnetic was concentrically aligned. Furthering on tests were done to eventually see displacements ranging from 1 – 5 mm.

After this time achievement, the setup had to be moved. Where, first a stationary interferometer, on a vibration table, was assembled with the Newegg laser. The interferogram was easily able to be resolved, but had a large amount of vibrations resulting in the interferogram losing alignment. Eventually this issue was resolved after fixing each component better. Afterwards the moveable mirror was mounted inside of a sample holder that was 3D printed. The sample holder was suspended above the right-angle mirror that directs the laser light vertically to what would be the moveable mirror. Several different 3D printed sample holders to adjust the center of mass.

Picture 2

In this configuration interferograms could be resolved, but the noise and drift caused the interferogram to quickly become miss-alignment. A SI-detector was mounted, equipped with a pinhole, so it would have the center of the interferogram, though most of the time the noise was sufficiently great to resolve the center of the interferogram. The noise was attempted to be eliminated with placing Styrofoam, bubble wrap, rubber pads, placing heavy masses on the base plate, and active noise cancellation near, under, and on the interferometer. Placing Styrofoam or bubble wrap under and or around the interferometer did not reduce noise a noticeable amount. Placing a heavy mass on the greatly decreased the noise to less than 12khz range. Placing additional support

underneath the sample holder did not result in any changes in noise. After the data was

collected to for Table of Stationary Interferometer. A sheet of printer paper and a copper

plate was place between the optical table and the interferometer's base plate of each run

to test the electrical continuity between the copper and the base plate of the

interferometer. The continuity tests showed only Run Numbers 4 and 5 had electrical
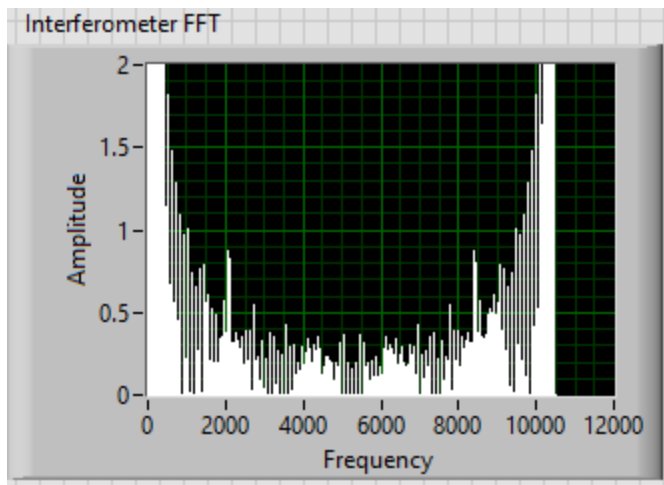
continuity.

Figure 14 shows the Fast Fourier Transform of the data collected from the stationary
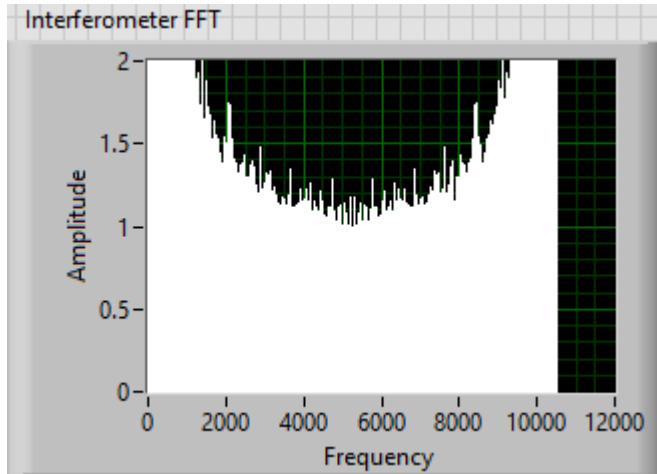
interferometer.

Figure 15 Displays the FFT of the signal of the stationary interferometer before noise
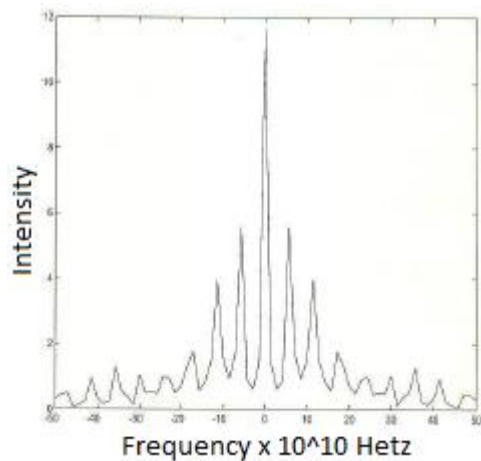
canceling efforts were taken.

Figure 16

Ashitkov et al. (2012) found similar noise as presented in Figure 16, but the

account for the level of noise detected.

The book written by Orfanidis (1995) offered a large number of possible noise

sources and methods to eliminate unwanted noise. Unfortunately, only the most basic

methods were able to noise cancellation methods were able to be used: attenuating,

buffering environmental noise, grounding mechanical noise.

Figure 14 shows the noise from the stationary interferogram. Table of Stationary Interferometer and Table of non-Stationary Interferometer show the results of the noise cancellation attempts.

Table of Stationary Interferometer			
Run Number	Number of Minimum(Min)	Number of Maximum(Max)	Ratio Min/Max
1	939	131	7.167938931
2	1032	558	1.849462366
3	1550	373	4.155495979
4	2572	3113	0.826212657
5	405	412	0.983009709

Table of Stationary Interferometer Run Number 1represents data collected from the stationary interferometer, with no noise cancellation efforts taken. Table of Stationary Interferometer Run Number 2 represents data collected from the stationary interferometer, with a rubber pad added, Styrofoam, and bubble wrap for support.

Table of Stationary Interferometer Run Number 3 represents data collected from the stationary interferometer with all possible noise sources; electronics removed from the table; and with a rubber pad added; Styrofoam, and bubble wrap for support.

Table of Stationary Interferometer Run Number 4 represents data collected from the stationary interferometer: a heavy metal block was added to the surface plate of the

optical path the interferometer rested on with all possible noise sources; electronics removed from the table; and with a rubber pad added; Styrofoam, and bubble wrap for support.

Table of Stationary Interferometer Run Number 4 represents data collected from the stationary interferometer a heavy metal block was placed on the surface plate of the interferometer.

The data collected suggests a large amount of vibrational noise was coming from the mechanical vibrations of the vibration optical table. In Table of Stationary Interferometer a rubber pad was added; Styrofoam, and bubble wrap were added between the interferometer and the vibration table and a heavy metal block was added on top of the base plate of the interferometer to eliminate in sources of vibrational noise, then the rubber pad added; Styrofoam, and bubble wrap were removed from and the heavy metal block was added on top of the base plate of the interferometer, then the ratio of minimum and maximum numbers of peaks improved.

Table of non-Stationary Interferometer				
Run Number	Number of Minimum(Min)	Number of Maximum(Max)	Ratio Min/Max	Distance (micro meters)
1	14083	10141	1.388719061	5
2	2346	13723	0.170953873	5
3	10537	2277	4.627580149	19

Table of non-Stationary Interferometer show a large variation in the number of peaks for the same distance traveled, and the data collected.

The data shown in Table of non-Stationary Interferometer and Table of Stationary Interferometer was collected between 1 am and 4 am, since more noise was present during normal business hours.

Results

The Watt Balance has a great amount of noise originating from the interferometer. Possible sources of noise are fluxuations in the surrounding air, air conditioning, electrical noise from the computer and power supply, vibrations from the floor.

The noise reduction techniques were not sufficient to produce a useable interferometer for a Watt Balance. Resting the interferometer's base plat on the optical table greatly reduced the noise. The unlimitable error warrants that the Watt Balance should be removed from the setup or attempt another method that would replace the functionality of the interferometer. Additionally, the setup should progress to integrating the controlled environment, IR, and Raman.

Appendix
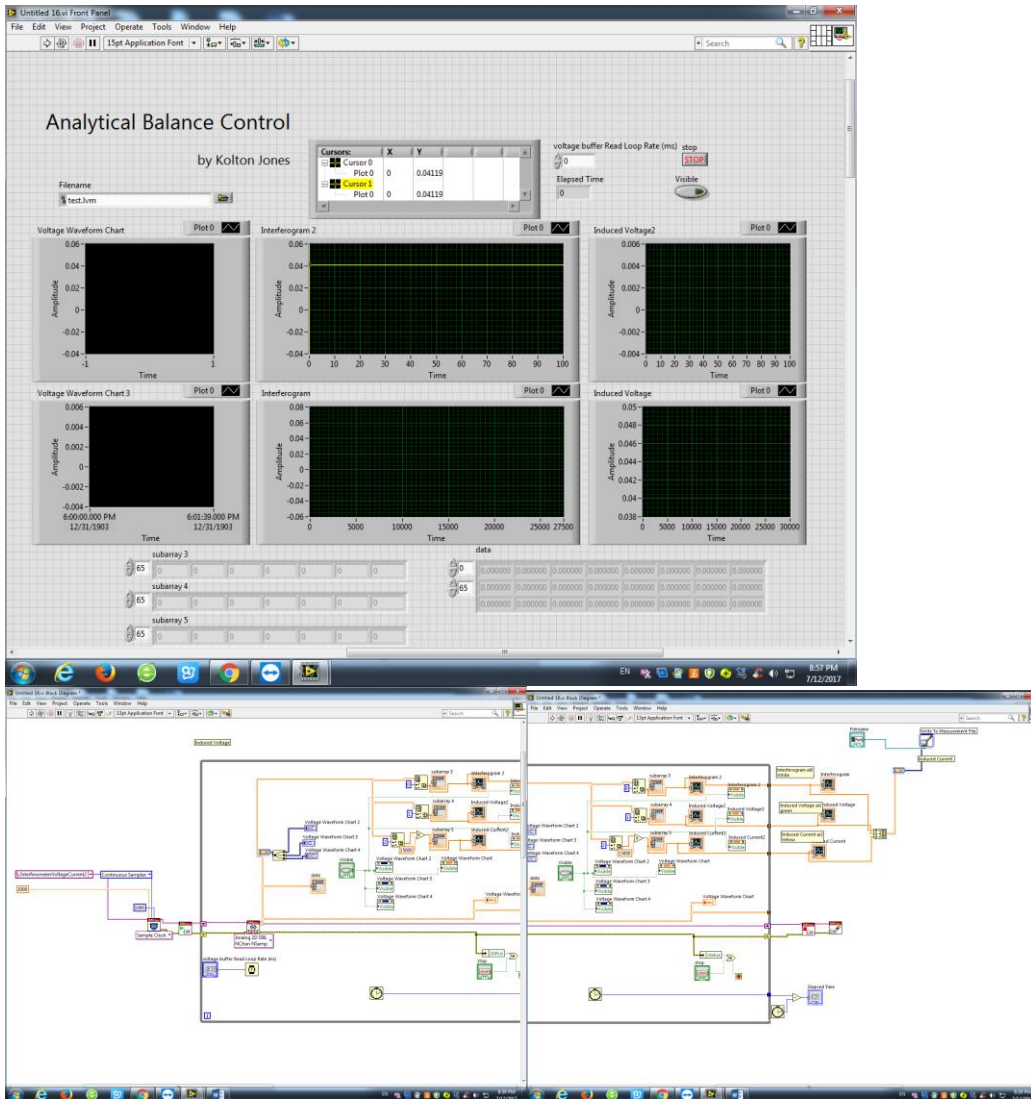
Bibliography Cited

InfraTec. (2014). *Advanced Features of InfraTec Pyroeletric Detectors*[Brochure].

　　　Author. Retrieved Summer, 2016, from http://www.infratec-

　　　infrared.com/fileadmin/media/Sensorik/pdf/Appl_Notes/Application_note_FP_de

　　　tectors.pdf

Ashitkov, S. I., Ovchinnikov, A. V., & Agranat, M. B. (2012). Interferometric

　　　measurement of melt depth in silicon using femtosecond infrared Cr:forsterite

　　　laser. *The African Review of Physics,*433-439. doi:10.1063/1.4739882

Chao, L. S., Schlamminger, S., Newell, D. B., Pratt, J. R., Seifert, F., Zhang, X., . . .

　　　Haddad, D. (2015). A LEGO Watt balance: An apparatus to determine a mass

　　　based on the new SI. *American Journal of Physics,83*(11), 913-922.

　　　doi:10.1119/1.4929898

Comnes, B., & Rosa, A. L. (n.d.). *Arduino PID Example Lab* . Lecture. Retrieved from

　　　https://www.pdx.edu/nanogroup/sites/www.pdx.edu.nanogroup/files/2013_Ardui

　　　no%20PID%20Lab_0.pdf

InfraTec. (2014). *Evaluation kit for Fabry-Perot detectors*(Tech.). Retrieved Summer,

　　　2016, from http://www.infratec-

　　　infrared.com/fileadmin/media/Sensorik/pdf/Appl_Notes/Evaluation_kit_for_Fabr

　　　y-Perot_detectors.pdf

Kibble, B. P., Robinson, I. A., & Belliss, J. H. (1990). A Realization of the SI Watt by the

　　　NPL Moving-coil Balance. *Metrologia,27*(4), 173-192. doi:10.1088/0026-

　　　1394/27/4/002

INPhotonics. (n.d.). *RPB Fiber Optic Raman Probe Low-cost Sampling Solution*(Tech.).

Retrieved Summer, 2016, from NPhotonics website:

http://www.inphotonics.com/probeRPB.htm 532 nm

Orfanidis, S. J. (1995). *Introduction to signal processing* (US ed.). Upper Saddle River,

NJ: Prentice Hall. doi:0132091720

Skoog, D. A., Holler, F. J., & Nieman, T. A. (2003). *Principles of instrumental analysis*.

London u.a.: Brooks/Cole.

Travis, J., & Kring, J. (2007). *LabVIEW for everyone: graphical programming made easy

and fun*(3rd ed.). Upper Saddle River, NJ: Prentice Hall.